Hundred-Picolitre Droplet on Demand Tape Drive and XES Prototypes for Time-Resolved Serial Crystallography at VMXi, Diamond Light Source

Pierre Aller[a,b*], Juan Sanchez-Weatherby[a,b*], Robert Bosman[a,e], Nicholas Devenish[a], Phillip Hinchliffe[c], Sam Horrell[a,b,f], Jophy Ip[a], Richard Littlewood[a], Andrew Male[a], Eva Giminez Navarro[a], Urszula Neumann[a], Jos J. A. G. Kamps[a,b,g], David Omar[a], Laura Parkinson[c], Muthraj Pandi[a], Nico Rubies[a], James Sandy[a], Anastasiia Shilova[a,h], Jim Spencer[c], Jonathan Spiers[a], John P. Sutter[a], Abbey Telfer[a], Amy J. Thompson[a], Catherine L. Tooke[d], Ben Williams[a,i], Tiankun Zhou[a,b], Michael A. Hough[a,b], Allen M. Orville[a,b^]

a Diamond Light Source Ltd., Harwell Science and Innovation Campus, Didcot, OX11 0DE, UK

b Research Complex at Harwell, Rutherford Appleton Laboratory, Didcot, OX11 0FA, UK

c School of Biochemistry and Cellular and Molecular Medicine, Biomedical Sciences Building, University of Bristol, Bristol BS8 1TD, UK

d Department of Biology and Biochemistry, 4 South, University of Bath, Bath BA2 7AY, UK

e University Medical Center Hamburg-Eppendorf (UKE), Hamburg, Germany (present address)

f Department of Life Sciences, Sir Ernst Chain Building, Imperial College London, London, SW7 2AZ, UK (present address)

g European Synchrotron Radiation Facility (ESRF), Grenoble, France (present address)

h Bruker UK Limited (present address)

i University of Oxford, Department of Statistics 24-29 St Giles, Oxford OX1 3LB, UK (present address)

*These authors contributed equally

^ corresponding author allen.orville@diamond.ac.uk

Synopsis We describe proof of concept experiments towards correlated serial crystallography (SSX) and X-ray emission spectroscopy (XES) from microcrystals at a microfocus synchrotron beamline. A droplet on demand tape drive system delivers microcrystals to the beam within picolitre volume droplets while XES allows validation of redox states of metals within protein crystals

Abstract Time resolved X-ray crystallography is experiencing a resurgence in part because of serial methods that readily allow scientists to create stop-motion movies of macromolecular function of photoactivation, enzyme catalysed reactions, and signalling pathways. While some reactions can be initiated with light, either naturally or using photocaged compounds, a more generally applicable approach is to mix microcrystals with reagents at varying time points prior to exposure to the X-ray

beam. A powerful approach has been to combine droplet on demand 'tape drive' sample delivery with X-ray emission spectroscopy (XES) that correlates atomic structure with electronic states of metal ions within the sample. To our knowledge, such a combined methodology has not been deployed previously at a synchrotron beamline and has been restricted to XFELs. Here we describe prototype experiments along the development pathway to a combined droplet on demand diffraction and XES system at the microfocus beamline VMXi at Diamond Light Source. We demonstrate the collection of a high-quality serial diffraction data set from microcrystals within picolitre volume droplets deposited on a moving tape. In separate experiments at VMXi, we collected XES data from microcrystals of a copper enzyme delivered using a high viscosity extruder. Together, these results demonstrate the feasibility of combined droplet on demand serial crystallography and XES experiments using a third-generation synchrotron beamline.

Keywords: Serial synchrotron crystallography (SSX), droplet on demand tape drive, X-ray emission spectroscopy (XES); metalloenzyme

1. Introduction

The emergence of X-ray Free Electron Laser (XFEL) facilities motivated serial femtosecond crystallography (SFX) data collection strategies including many sample delivery methods that are amenable to time-resolved studies (Barends et al., 2022; Branden & Neutze, 2021; Chapman, 2019). Benefiting from a collaborative community and exchange of ideas, serial crystallography is becoming an increasingly popular tool for structural biologists especially at synchrotrons where beamtime is more readily available than is the case at XFEL sources (Aller & Orville, 2021; Orville, 2020; Pearson & Mehrabi, 2020). Third and fourth generation synchrotron beamlines, with their high flux and microbeam capabilities, are particularly well-suited for serial crystallography (Jaho et al., 2024; Mehrabi, Schulz, Dsouza, et al., 2019) especially with the advent of diffraction limited lattices (so called "fourth generation" synchrotrons), which enable even smaller beam sizes and significantly greater flux densities. Several beamlines are now fully dedicated to performing serial crystallography such as ID29 at ESRF-EBS (Orlans et al., 2025), T-REXX at PETRA III (Mehrabi, Schulz, Agthe, et al., 2019) and MicroMAX at MAX IV(Gonzalez et al., 2025).

At Diamond Light Source, two macromolecular crystallography beamlines are particularly suitable for serial crystallography: I24 and VMXi. The micro-focus beamline I24 has developed a world leading, flexible sample mounting / delivery environment that enables both rotation and serial data collection by easily switching set-up between "pin" mode and

“serial” mode. I24 is used for serial data collection using either a fixed target setup or a high viscosity extruder (Birch et al., 2023; Jaho et al., 2024). On the other hand, VMXi was designed for *in-situ* room temperature data collection from crystals within crystallisation plates. VMXi is well suited for serial data collection since it incorporates a multi-layer monochromator (DMM) resulting in high flux (>2×10^{13} ph/s at 16 keV) with a microfocus pink beam (10 ×10 µm) with broad energy bandpass (~5×10^{-3} ΔE/E) (Sanchez-Weatherby et al., 2019; Sandy et al., 2024). The characteristics of VMXi make it ideally suited for serial crystallography in term of flux, beam size and detector repetition rate (Eiger2X 4M, running in continuous mode at 500 Hz).

Time-resolved crystallography studies typically require interpreting electron density maps of reaction intermediates that often present ambiguities, which may or may not be easy to resolve from the electron density alone. Consequently, complementary spectroscopic methods are particularly valuable for time-resolved studies since they can provide additional orthogonal data to help resolve ambiguities, especially if the spectroscopic data comes from the same sample and X-ray pulse. Combining serial crystallography with X-ray emission spectroscopy (XES) is perhaps the most highly correlated strategy for simultaneously obtaining two types of data from the same sample and X-ray pulse/exposure (Fuller et al., 2017; Kamps et al., 2024). Thus, XES data can validate the interpretation of electron density maps, especially for metal centres within metalloenzymes and in time-resolved experiments.

The most optimal way to collect XES while simultaneously collecting diffraction images, uses a spectrometer in a von Hamos geometry spectrometer, located at ~90 to the beam direction. Developed for XFEL applications, a consortium including ourselves have demonstrated the drop on tape method (DoT) combining at the same time XES and diffraction experiments (Butryn et al., 2021; Kamps et al., 2024; Rabe et al., 2021). The DoT strategy, originally developed at a synchrotron facility as described previously (Roessler et al., 2013), is now predominantly employed at XFELs (Fuller et al., 2017). Meanwhile, alternative tape-based sample delivery methods—such as those using capillaries to produce continuous sample streams—are being actively developed and utilized at synchrotron sources (Kamps et al., 2024). The main advantages of the DoT sample delivery system are i) the low sample consumption since the nanolitre droplets of sample are ejected on demand and then synchronized with the X-ray pulse compared to jet techniques which dispense sample between X-ray pulses, ii) versatility of the sample delivery method allowing several reaction initiation methods such as turbulent mixing, gas diffusion, and light illumination (Kamps et

al., 2024) and iii) possibility to work under anaerobic conditions (Lebrette et al., 2023; Rabe et al., 2021). On the other hand, the currently available DoT system is bulky, complicated to install and requires several trained operators to work. It also uses 1-5 nanolitre size droplets and we note that a system with the capability to work with smaller droplets would significantly reduce sample consumption. The Center for Free-Electron Laser Science (CFEL), Hamburg, subsequently developed a simpler tape drive (CFEL TapeDrive 2.0) operating reel to reel and using microfluidics to mix micro-crystal slurry with ligand/substrate before depositing a streak on the moving Kapton® tape (Beyerlein et al., 2017; Henkel et al., 2023; Zielinski et al., 2022). This tape drive is used at P11 (Petra III) and MicroMAX (Max IV) and a similar tape drive exists at ID29 (ESRF-EBS). The main limitation of this system is the lack of versatility for implementation of complementary methods.

XES of metal containing proteins is an element selective technique which allows for electronic properties (*i.e.* redox and spin states) to be explicitly measured following ejection of a core electron (Cutsail & DeBeer, 2022; Glatzel & Bergmann, 2005). For 3d transition metals including copper, the three most relevant XES lines are the Cu $K\alpha_{1,2}$ (2p-1s), Cu $K\beta_{1,3}$ (3p-1s) and valence to core (Cu $K\beta_{2,5}$) in decreasing order of their signal intensity. Cu $K\alpha_{1,2}$ is a reporter of oxidation state while Cu $K\beta_{1,3}$ is sensitive to metal-ligand covalency, spin state and oxidation state. The weakest (valence to core) signal can offer insights into ligand binding and the nature of valence molecular orbitals but is highly challenging to measure. XES coupled with serial crystallography has been used to monitor the oxidation state of functionally critical metal centres. In isopenicillin N-synthase (IPNS), time resolved XES with high resolution SFX identified specific structural intermediates after oxygen was used to initiate reactivity with the ACV substrate. The width of the Fe $K\alpha_{1,2}$ peak as a function of reaction time identifying the correct time point in the SFX data collection at which a crucial intermediate had formed (Rabe et al., 2021). Similarly, in the case of methane monooxygenase Fe $K\alpha_{1,2}$ XES data were similarly used to identify catalytic intermediates after reaction initiation (Srinivas et al., 2020). A third example used manganese Mn $K\beta_{1,3}$ XES to follow the S2 → S3 transition in photosystem II (Ibrahim et al., 2020).

One important aspect for our tape drive development programme is the association with XES. Metal containing proteins are particularly prone to X-ray induced radiation alterations, which can beneficially promote mechanistically relevant reactions, e.g. in redox proteins and enzymes, and/or lead to redox state changes and experimental artefacts that may compromise the experimental outcome (Beitlich et al., 2007; Chreifi et al., 2016; Hajdu et al.,

2000; Pfanzagl et al., 2020). Additionally, it can be challenging to identify conditions and timepoints where particular catalytic intermediates have built up to high occupancy. Spectroscopic measurements from crystals provide highly complementary information. There is added value if/when experiments are fully correlated such that the different data types emerge from the same microcrystal volume responsible for the diffraction pattern, with the additional data supporting the interpretation of the electron density maps and refined atomic model(s). Serial crystallography helps to mitigate the X-ray induced damage in the sample by spreading the X-ray dose over typically thousands of microcrystals. Our goal for the new instrument is to exploit XES signal at both synchrotron and XFEL beamlines.

Here we describe proof of concept results from prototype testing of different components of the DoT with XES instrument under development at VMXi at Diamond Light Source. Serial crystallographic data measured from protein microcrystals within 150 pL droplets on a moving Kapton® tape are described. From a second experiment, XES results for copper $K\alpha_{1,2}$ measurements are described from protein microcrystals using 4 analyser crystals out of the 16 planned in the final design with sample delivery using a viscous extruder. These results indicate the feasibility of carrying out this combined approach at a microfocus synchrotron beamline.

Our key design requirements were therefore to keep the tape drive simple to use, transportable, and compact due to the space constraints at VMXi with the goal of portability to enable experiments at other beamlines. The installation of the prototype of the tape drive at VMXi demonstrated the ability to successfully obtain good quality serial crystallography data at high resolution, from microcrystals of serine beta lactamase CTX-M-15. The von Hamos XES spectrometer prototype allowed measurements of representative Fe and Cu $K\alpha_{1,2}$ spectra of salts and copper nitrite reductase (CuNiR) microcrystals, respectively. These results provide proof of concept that combined DoT/XES data collection will be feasible at a third-generation synchrotron source, with further improvements expected at the diffraction limited Diamond-II (https://www.diamond.ac.uk/Diamond-II.html) or at XFELs.

2. Methods

2.1.1. Sample preparation for tape drive experiments

Recombinant His-tagged CTX-M-15 was expressed and purified as previously described (Tooke et al., 2019). CTX-M-15 microcrystal slurries were generated as previously described (Butryn et al., 2021), using crystal seed stock that was generated by crushing macro-crystals grown by sitting drop vapour diffusion (Tooke et al., 2019); protein (5 µL) was mixed with crystallisation solution [5 µL; 2.0 M $(NH_4)_2SO_4$, 0.1 M Tris pH 8] and seed (5 µL), and equilibrated against crystallisation solution (500 µL) in 24-well sitting drop plates (Hampton). Rod-shaped crystals grew within 24 h, with a maximum width of 3-8 µm and length around 8 µm. Crystal density was ~1 x 10^8 crystals mL^{-1} as measured using a TC20 automated cell counter (BioRad) or a counting chamber (Neubauer).

2.1.2. VMXi instrumentation setup and installation of tape drive prototype

The tape drive prototype consisted of a motor and tape, wash-dry mechanism, and sample ejection system (Fig. 1). First, the system was installed and aligned to the VMXi X-ray beam path. The typical layout of the beamline has been described previously (Sanchez-Weatherby et al., 2019; Sandy et al., 2024). In standard VMXi operation, the X-ray beam is focused on the rotation axis of the beamline goniometer (Fig. S1a). Due to the space requirements of the tape drive system the sample interaction point for the experiments described here was instead placed 250 mm downstream from the standard position by modifying the settings of the microfocus bimorph mirrors (Fig. S1b). An extension tube was made to visualise the beam at the newly created reference point using a drilled lens to allow the X-ray beam to pass through. In this way the beamline on-axis viewing system could be re-used at this new focal point and the beam could be re-focused through the lens onto a YAG screen at the new downstream sample position. The tape drive system was aligned to the focused beam by referencing with the on-axis viewing camera, such that the interaction region is aligned with the focal point of the X-Ray. A secondary camera was placed orthogonal to the sample position that allowed monitoring of the sample position vertically and horizontally on the tape width while collecting diffraction data. An aluminium breadboard (MB2060/M, Thorlabs) mounted on MiniTec framework above the VMXi goniometer enabled the installation of the prototype tape drive as shown in Fig. 1a.

Droplet Ejection system.

Previous DoT tape drive systems utilized acoustic droplet ejection (ADE) to dispense 1–5 nL droplets containing microcrystals onto a moving Kapton® tape (Hadimioglu et al., 2016;

Soares et al., 2011). To achieve lower sample consumption, we employed a piezoelectric injector (PEI) newly developed by PolyPico Technologies Ltd. (Cork, Ireland) (Miniature Dispensing Head). This device can dispense individual micro-crystal-containing droplets in the range of 50–150 pL at a rate of up to 50 kHz. The reduction in droplet volume significantly decreases sample usage and will improve signal/noise ratio but makes dehydration effects more prominent. To minimise dehydration, we positioned the ejection as close as possible to the interaction point (~ 60 mm), but future designs will incorporate a controlled humidity environment to avoid any issues.

The droplet ejection module comprised (i) the PEI head and sample cartridge (used to hold the crystal slurry); (ii) the sample camera and the strobe LED (used to visualise ejection) iii) the wide-angle camera (used to monitor sample consumption) (Fig. 1c). For longer duration experiments the PEI cartridge was fed fresh samples via a fused silica capillary (with inner diameter of 150 µm) using a remote-controlled precision 250 µL syringe pump (KDS Legato™ 130) sitting on a rocker to prevent sample settling in the syringe. Only the minimum amount of sample (10-20 µL) is maintained in the cartridge preventing crystal settling and clogging of the cartridge aperture.

Tape drive and wash-dry mechanism

The prototype belt drive utilised a brushless DC motor (MAXON) to power the conveyor belt made of Kapton®, 60 mm wide and 50 µm thick (kb RollerTech). The Kapton® tape was treated with *Rain Repellent* (RainX) to make the surface hydrophobic thus improving drop adhesion and shape. The moving tape was cleaned after the interaction region by passing through a 3D printed module designed to pressure wash and air dry the tape before it was re-injected with sample (Fig. 1b). Although the tape drive can be operated at higher speeds for this study, we restricted the speed to 25 mm/s to ensure effective tape cleaning with this early design wash/dry system. This speed allows for 700 µs exposure (for an 8 µm crystal traversing the 10 µm X-ray beam) suitable for this application. We anticipate using a wide range of tape speeds in the final design of the tape drive (Table 1).

Synchronisation and X-ray data collection

Experiments at XFEL beamlines typically rely on the pulse generated by the source as their master clock for synchronisation. In these synchrotron experiments synchronisation was achieved by using a local waveform generator (33600A, Keysight) instead to create a TTL pulse at the desired frequency up to 500 Hz (Fig. 2a). This master signal was used to trigger

the PEI ejection of the samples onto the tape and a delayed signal from this master was used to strobe an LED (4 V white, 5mm) to monitor the point of contact of the droplet with the tape. The droplets that travelled on the tape to the interaction region with X-rays were visualised using one on-axis viewing camera and one orthogonal camera and were illuminated by a strobed LED behind the tape (Fig. 1c) (preventing any shadowing on the diffraction images). The strobed LED (behind the tape) illuminated the interaction region to determine the point at which the droplets traverse the beam by fine adjustment of the delay and pulse width of the LED strobe. The adjusted TTL pulse was then used to trigger detector data collection. This ensured that data collection was started just before the sample met the beam and that the exposure time ended just after the drop passed through the interaction zone. This mechanism will allow us to maximise the signal to noise (by minimising the exposure time without a droplet in the beam) and adjust the trigger point to correct for any slight alterations in ejection and tape movement. Future iterations of the device will also use this technique to control a second ejection point where compounds will be mixed with the droplets on the moving tape, thus initiating chemical mixing, but it was not tested during the experiment described here.

2.1.3. Data collection

For data collection the linear tape speed used was 25 mm/s, which means that a crystal with the maximum dimension around 8 µm spent a maximum of 700 µs in a 10 µm X-ray beam, which is the equivalent of a dose of 12 kGy per crystal. The PEI dispensed on the edge of the Kapton® tape droplets containing CTX-M-15 microcrystals at a frequency of 100 Hz enabling the acquisition of a full dataset of >20,000 indexed images in about 30 min. The ejected droplet volume depends on several parameters such as the aperture of the PEI cartridge and the amplitude and width of the signal controlling the ejection. The droplet velocity and volume were changed by increasing both amplitude and width of the signal. In normal operation the droplet velocity before touching the tape was about 1-2 m/s. We used a PEI aperture of 100 µm to avoid clogging the cartridge with the microcrystal slurry. The amplitude and width of the ejection signal were adjusted to deliver a droplet with a volume of about 150 pL. While the droplets were dispensed at 100 Hz the detector collection rate was 500 Hz, which corresponds to a maximum of 2 ms exposure time (Fig. 2b). The Eiger2X 4M detector was positioned at 230 mm from the sample position, allowing a resolution of 2.4 Å in the inscribed circle and 1.72 Å in the corner of the detector. The X-ray beam was of 16 keV energy and focused to 10×10 µm^2 with a flux of 2×10^{13} photon/s.

2.1.4. SSX data processing

CTX-M-15 serial synchrotron crystallography data were processed using xia2.ssx (Beilsten-Edmands et al., 2024), (Table 2). Individual data files from data collection runs underwent spotfinding, indexing and integration using xia2.ssx. The output data files from each run were scaled and merged using xia2.ssx_reduce. The additional scaling parameter weighting.error_model.basic.min_Ih=300 was required to improve error modelling due to varied intensity distributions. A minor additional unit cell population was removed using unit cell clustering via the parameter clustering.threshold=5. Analysis of the indexed data versus frames collected suggested an approximate indexed hit rate of 10%. The structure was solved using PDB 7BH6 as the initial model. Structures were completed through rounds of iterative refinement in phenix.refine (Adams et al., 2010) and manual model building in Coot (Emsley & Cowtan, 2004), and validated by Molprobity (Chen et al., 2010) and Phenix.

2.2. X-ray emission spectroscopy instrumentation at VMXi

A compact von Hamos spectrometer to measure XES was developed in house at Diamond and implemented on beamline VMXi consisting of three key components: sample interaction zone, analyser crystal/s array and a 2D X-ray sensitive detector, Fig. 3. Because VMXi had been designed as a high throughput *in situ* crystallography beamline with limited access and a small hutch, several factors constrained the available options for XES experiments. The geometry was chosen to capture the emitted fluorescence orthogonal to the main beam path, diffracted down on to a detector below the sample position. The bending radius of the crystals was 400 mm giving the best balance between capturing a large solid angle within the available space and preventing clashes with existing equipment. For the proof-of-concept experiments described here we used four 110×25mm Si (111) crystals arranged in a vertical block with 6 mm spacing between crystals at ~ 90° in von Hamos geometry to collect Cu $K\alpha_{1,2}$ XES lines with the Si(444) reflection. To measure Fe $K\alpha_{1,2}$ XES we instead used two Ge(440) analyser crystals from XRSTech with a working distance of 250 mm.

The focusing axis along the horizontal plane and the Bragg plane was vertical, Fig. 3. Analyser crystals were aligned to produce vertical lines on the detector. The analyser crystals could be independently adjusted in focal length, pitch and yaw in order to overlay the resulting signal thus improving signal to noise. This adjustment was carried out by “eye” using reference metal foils or chemical solutions, but future systems are likely to include an

automated calibration routine to ensure consistent setup. The X-ray detectors used for these proof-of-concept XES experiments were a Merlin 1M (Plackett et al., 2013) and a Tristan 1M (Omar et al., 2022) TimePix3 (Poikela et al., 2014) detector of active area 113.8 × 28.3 mm (2048 × 512 active pixels each of 55 × 55 μm) for the Fe and Cu signals, respectively. We used the pre-existing downstream interaction point (using the extended on-axis-viewing system and re-focused beam) but required a different supporting structure to include the von Hamos crystal array and the Tristan detector.

2.2.1. Sample preparation for XES

Metal containing salts were used in the dry chemical form. Microcrystals of AcNiR were prepared as previously described (Horrell et al., 2016) and their size and density assessed by visible light microscopy. Crystals of AcNiR were tested for diffraction quality by mounting between two layers of mylar for data collection at Diamond I24 before transfer into a high viscosity medium for extrusion. Two parts of AcNiR microcrystals slurry were mixed with three parts of monoolein (HR2-435, Hampton Research) to form the lipidic cubic phase (LCP) prior to loading in the high viscosity extruder.

Iron and copper containing salts [$Cu(I)Cl_2$ (229628, Merck), $Cu(II)Cl_2$ (222011, Merk), $K_3Fe(CN)_6$ (10266370, Fisher Scientific) and $K_4Fe(CN)_6$ (11452378, Fisher Scientific)] were used as solids mounted between O_2 tight foils using standard chip-less chips (Doak et al., 2018). Iron foil used for standard was purchased from Advance Research Materials Limited (FE163808).

2.2.2. Data collection

For these experiments simple mounting solutions were utilised in order to mount different samples on the beam path. Standard calibration metal foils held using kinematic posts were oriented at 45° to the X-ray beam to ensure a single source point to improve resolution and focus of the signal onto the 2D Tristan X-ray detector.

Sample delivery for protein microcrystals were ejected to the interaction point using a high viscosity extruder and “catcher” (Weierstall et al., 2014). This delivery system was used as it was very simple to install and align, albeit with higher background and not permitting synchronisation of data.

Non-active areas of the XES detector were masked with lead tape (5 mm thick) to avoid contamination of the signal from scattering of X-rays by equipment at the beamline near the interaction region. A helium filled cone, arranged such that the air absorption path was reduced to only 10 mm, was used to improve signal to noise, Fig. 3c. The LCP was extruded at a rate of 2 to 5 nanolitres per minute through a nozzle size of 75 μm inner diameter. The flow rate of the ejector was varied to ensure a stable flow, resulting in an absorbed dose range of 12-35 kGy depending on the flow rate. X-ray diffraction data (not shown) were also measured simultaneously with the XES data and diffraction detector frames were used to produce frames from the event counting Tristan detector.

2.2.3. Data processing

XES data recorded either on the Merlin 1M or on the Tristan 1M detector were processed using in-house developed software, SEDEA (Serial Energy Dispersive Emission Analysis). Raw XES data were converted into a set of images that matched the X-ray diffraction frame number or 30 images for foil/salt data. Hot pixels were removed with a given intensity threshold. A region of interest (ROI) around the spectrum was selected and pixel intensities along the y-axis (vertical) were summed to produce the raw spectrum. Pixel intensities in two thin bands beyond and below the ROI were also vertically summed as background and subtracted from the raw spectrum. The intensity of the background-subtracted spectra was normalised to the maximum intensity, which was as expected the maximum of the $K\alpha_1$ peak. The raw XES data collected is a function of pixel number, therefore an energy calibration is required. For the Fe data $K\alpha_{1,2}$ XES data was measured on an Fe foil preceding the measurement of the samples (Fig. S2), which allowed the conversion of pixel numbers to energy (eV) using known $K\alpha_{1,2}$ emission lines (Thompson et al., 2009). For the Cu data, $CuCl_2$ data was measured using the experimental set up reported and this data was energy calibrated using $CuCl_2$ data collected on I20-Scanning at Diamond Light Source by Dr Sherwin (University of Oxford).

3. Results

3.1. Tape drive operation and delivery of droplets

Having tested several alternative moving sample support structures (reel to reel tape, rotating disk, flying droplets, data not shown) we established that a closed loop of moving Kapton® belt drive, as used previously in the DoT LCLS system, was the best performing option. Nevertheless, as we wanted to use much smaller droplets, here we needed a more precise mechanical performance, very tight motion control and highly precise ejection. Achieving the required performance necessitated the development and testing of several iterations of the tape drive system and its associated wash-dry mechanism. The version used in the present study represents an intermediate design—less precise than the final design, yet sufficiently robust to enable proof-of-concept experiments at VMXi.

First, the capability to consistently position droplets on the moving tape and synchronise this with X-ray exposures was tested. X-ray diffraction data were collected to 1.83 A resolution from CTX-M-15 microcrystals within droplets on the tape using a linear tape speed of 25 mm/s. When the PEI was positioned 60 mm from the interaction region, it took 2.4 s for the microcrystal-containing droplet to reach the X-ray beam. In this configuration, the resulting diffraction patterns were of good quality and were successfully processed (Fig. 4a). However, when the PEI was placed more than 100 mm away, no diffraction patterns were observed, likely due to dehydration effects under a relative humidity of 20% maintained in the VMXi hutch.

To ensure the X-ray beam consistently intersected with the droplets on the tape, we implemented a data collection strategy in which droplets were ejected at 100 Hz, while the detector acquired frames at 500 Hz with a 2 ms exposure time (Fig. 2b). Active feedback was provided by monitoring the acquired image size. When a droplet was hit by the X-ray beam the resulting image size was larger due to the solvent ring scattering compared to an image where a droplet was not hit by the X-rays. We used this tool to move the tape as close as possible to the X-ray beam until we observed a pattern corresponding to a larger image 1 in every 5 collected (Fig. S3). By combining this approach with a Kapton® tape positioned slightly off axis relative to the X-ray beam, we ensured that the beam grazed the tape surface, even larger images are observed when the beam intersect with the tape. This geometry minimised tape-induced background scatter in the diffraction data, unlike the configuration used by the DoT which requires tape background correction tools (Fuller et al., 2017).

The main advantage of using the PEI for ejection of droplet containing microcrystal slurry is to reduce sample consumption. Indeed, the PEI eject droplets of around 150 pL while the DoT using the ADE method (Fuller et al., 2017; Hadimioglu et al., 2016) produces droplets in

the range of 1 to 5 nL depending on the working frequency of the transducer. The droplet size generated by the PEI depends on the cartridge aperture. For CTX-M-15 we used a 100 µm aperture to avoid clogging at the tip of the cartridge and to create droplet volume around 150 µL. The data collection time was 32 min, which means with a droplet ejection frequency of 100 Hz, we used less than 50 µL of micro-crystal slurry (with a density of 10^8 crystals mL^{-1}) for a high-quality dataset. The sample consumption is comparable to the fixed target approach (Horrell et al., 2021; Jaho et al., 2024) . With ADE, for a similar number of indexed lattices (~20,000) and a better indexing rate of 20% we would require at least 250 µL of the same slurry.

During the 32 min data collection, 192,000 droplets of 150 pL volume containing CTX-M-15 microcrystals were ejected with an average of 15 crystals in each droplet, according to a crystal density of 10^8 crystals mL^{-1}. With a 10 % hit rate we indexed 20,556 lattices. In total we dispensed about 3,000,000 crystals corresponding to 0.4 mg of protein.

The SSX data produced a clearly interpretable electron density map to 1.83A resolution (Fig. 4b) and refined structure, table 2, from an estimated exposure time of 700 microseconds (12 kGy per crystal).

4. XES data

During these prototyping experiments we used two different 2D X-ray sensitive detectors to measure XES. For our initial tests for Fe signal (due to its smaller footprint and ease of use) experiments were carried out with a 1M Merlin photon counting detector. Once the experiments progressed further, we moved to using a 1M Tristan event counting detector. The use of this type of detector brings advantages for the combined tape drive/XES experiment as it permits recording the data as a time stream with 6 ps resolution. This data can later be re-processed to re-construct data around the time points where droplets traverse the beam path, thus allowing removal of data at timepoints when only noise is being recorded allowing the signal to noise to be maximised despite not having a pulsed X-ray source. For these studies we tested this detector but for the data presented here we did not optimise data sampling in this way but the plan for the future is to build the system with a custom 2M Tristan detector that should enable the system to record very clean spectroscopic data.

To test the feasibility of XES data collection at a microfocus synchrotron macromolecular crystallography beamline we initially used an iron foil and iron salts to

measure the Fe Kα signal using two analyser crystals (Ge440) curved to work at a short 250 mm (due to analyser crystal availability). Fe $K\alpha_{1,2}$ spectra were obtained from potassium ferricyanide $K_3Fe(CN)_6$ and potassium hexacyanoferrate $K_4Fe(CN)^6$ salts in solid form. Strong spectra and a clear difference between the spectra of the two different salts, containing two different oxidation states of iron, were observed, Fig. 5a.

In subsequent experiments we used a new subset of 4 analyser crystals cut to a 400 mm curvature (working distance of the planned final design of the instrument), to measure Cu $K\alpha_{1,2}$ XES data. The spectra of $Cu(II)Cl_2$ and $Cu(I)Cl_2$ salts in solid form, showed good signal to noise and distinct from each other, Fig. 5b.

Finally, we measured XES spectra from protein microcrystals. Crystals of copper nitrite reductase from *Alcaligenes cycloclastes* (Horrell et al., 2018) were injected into the X-ray beam in an LCP medium using a high viscosity extruder. For these tests we used the extruder as it was better characterised and frequently used in serial crystallography experiments. although it was expected to produce weaker XES signals due to higher background than will be the case from similar microcrystals in pL droplets of the future tape drive. Despite this, in the resulting spectra from protein microcrystals, both peaks in the Cu $K\alpha_{1,2}$ signal were well resolved and clearly distinct from each other, fig 5c. Copper nitrite reductase contains two copper ions per 37 kDa monomer of the functional trimer. These copper ions have different function and active site ligation which may lead to differences in their rate of X-ray reduction, the resulting XES spectrum here is an average of the signals from both copper environments, which are different from each other.

4. Discussion

Our proof of principle experiments yielded two main outcomes (i) collection of diffraction data was possible from microcrystals dispensed onto a moving tape using 150 pL droplets and (ii) Cu K_α XES spectra from enzyme microcrystals delivered using a high viscosity extruder could be measured using the von Hamos system. In both cases, despite being in the early developmental stage of the project, good quality data were obtained. This provides confidence that the final system will be able to deliver a strong capability, by combining both of these complementary measurements. Using the prototype a crystal structure was determined using less than 50 µL of microcrystal suspension. We collected the data in about 30 minutes producing 20556 indexed diffraction images to 1.83 Å resolution. The SSX

structure was similar to that obtained from experiments at SACLA (drop on tape, PDB 7bh3), PAL-XFEL (fixed target, to be published), I24 (fixed target, to be published), and a single crystal structure determined at 100 K (PDB 4HBT). The major difference between structures is a slight movement of one of the key catalytic residues (particularly room temp vs 100 K) - Lys73 - and of the catalytic water; otherwise, the overall structures are similar with Cα RMSDs against the VMXi structure (calculated using PDBeFold) of 0.1 (SACLA, DoT, room temperature), 0.14 (PAL-XFEL, fixed target, room temperature), 0.18 (I24, fixed target, room temperature) and 0.2 (100 K structure).

For this proof of concept work we focused on creating a simplified tape drive mechanism to confirm that it was possible to dispense samples as droplets of 150 pL volume onto a moving tape, then present them to the X-ray beam and record diffraction data at a synchrotron beamline. At VMXi the challenge of matching/synchronising the sample to the beam is slightly different to that at XFEL sources. The synchrotron beam is not pulsed (hence guaranteeing the presence of X-rays at the time the droplet crosses the interaction point) but the dose rate is much smaller and dependant on the tape velocity (making synchronisation by *e.g.* following the explosion of droplets as a result of X-ray exposure, typically used at XFELs, more difficult). At XFELs the X-rays and the detectors are already synchronised, so the challenge is limited to synchronising the samples to the pulse by adjusting the ejection delays by using the master clock of the source. The confirmation of correct synchronisation can be achieved by visual observation of droplet destruction by the beam or by observing the scattering of the droplets in the X-ray diffraction data. In the case of the synchrotron this is not as simple, the lack of a pulse to follow means that the detector and the samples need to be synchronised in order to select the appropriate data collection time when the crystal-containing droplet traverses through the constant beam. If this is not done correctly although diffraction will probably be recorded the level of background scattering caused by the constant beam would limit the signal to noise of the data. For these reasons, we had to develop effective ways of synchronising samples and detector so that we could optimise the data collection event to the point of maximum signal/noise ratio, as described here.

We expect the final design to deliver a much greater control and sensitivity making these sorts of experiments more routine and providing a useful asset to the time resolved structural biology community. We will use coordinated trigger signals and gating of the X-ray detector to measure diffraction data only when a droplet is traversing the beam, greatly improving signal to noise and allow for shorter exposure times. It is notable that in this study

we obtained excellent quality diffraction data even without this improvement. Another aspect the final system will improve is humidity control (to avoid dehydration of samples) and controlled anaerobic conditions (final lower concentration not yet established) to permit data collection from oxygen sensitive microcrystals. As demonstrated here, reducing the droplet size (from 5 nL down to 0.15 nL) using PEI compared to previous ADE systems greatly reduces the quantity of sample required to measure a dataset, increases the signal strength and shortens the mixing times when executing drop on drop experiment. The constant but weaker X-ray source of the synchrotron compared to the near instant 10-50 fs pulse duration at an X-FEL, despite posing a challenge with signal and background, is also beneficial for reducing the quantity of sample needed as passing droplets through a beam that is always-on provides greater opportunities for the interaction of the crystals with the beam that may yield data.

The results with the prototype XES system are also very promising. In this proof of principle experiment we only used a reduced solid angle (only up to 2 or 4 von Hamos analyser crystals out of the planned 16 in the final design). Furthermore, the sample delivery available at the time, LCP extruder, was far from ideal as it is difficult to control and produces large background leading to much weaker signal to noise. The final version of the device will measure XES from 150 pL droplets and record the data using the newly developed Tristan 2M event counting detector. The final crystal array is planned to comprise of 4 sets of 4 analyser crystals (110 $\times$ 25 mm) cut and positioned such that the emitted fluorescence from the sample is diffracted back onto the 2D detector. The crystals are placed orthogonal to the beam path and aligned such that on the vertical plane the lattice spacing creates a discrete diffraction point on the detector depending on the energy. By selecting crystals with different lattice parameters, the device can be used to observe up to 4 separate $K\alpha_{1,2}$ emission lines (planned to be used to detect Fe, Cu, Mn and Ni spectra) or, if all 16 crystals are used, we plan to be able to analyse $K\beta$ spectra for the same elements. On the orthogonal plane the crystals are bent such that the X-rays emitted are focused along the horizontal plane improving the signal to noise of the instrument. This creates a spectral line or lines where each point represents a discrete energy.

Energy calibration of the Fe and Cu $K\alpha_{1,2}$ XES spectra using the methods reported in 2.2.3 gave an energy axis with an energy resolution of 0.1 eV, which we anticipate being adequate for tracking changes to spin state and oxidation state changes across a time resolved

series of XES measurements. The $K\alpha_{1,2}$ XES spectra for the iron salts [$K_3Fe(CN)_6$ and $K_4Fe(CN)_6$] are congruent with literature values for both the $K\alpha_1$ FWHM and centre of mass (COM) (Lafuerza et al., 2020) (Table 3). The successful measurements of both Fe and Cu $K\alpha_{1,2}$ XES demonstrate the versatility of the von Hamos spectrometer for element specific spectroscopic measurements by interchanging suitable analyser crystals. As expected, the Cu $K\alpha_{1,2}$ XES spectrum for AcNiR has a lower signal to noise ratio when compared to the salt spectra however it is promising that the signal to noise of the protein spectrum is sufficient to calculate $K\alpha_1$ FWHM and COM which could be used to track changes in the oxidation state across a time resolved reaction series. The signal to noise ratio for protein $K\alpha_{1,2}$ XES spectra is expected to improve with the aforementioned planned advances to the sample delivery system and von Hamos spectrometer.

In summary, these proof of principle experiments demonstrate the feasibility of a synchrotron-based instrument combining droplet on demand and XES for routine easy to use time resolved crystallography. To respond to the challenges encountered in this study a device is being designed and built to collect concurrent structural and spectroscopic possible to in a time-resolved manner under controlled environmental conditions.

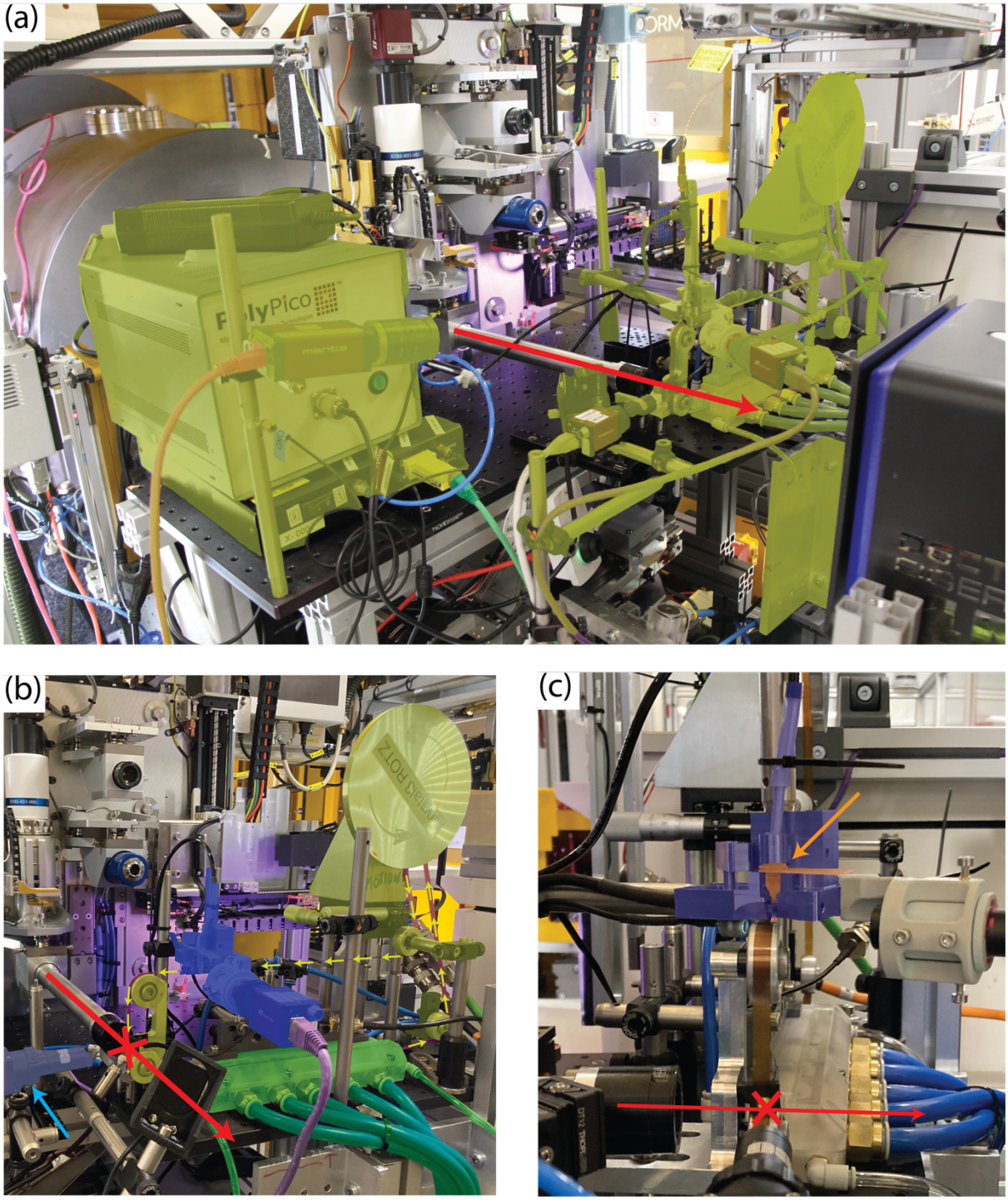

Figure 1 Tape drive prototype at VMXi. (a) Overall view of the installation of the tape drive prototype at the VMXi beamline. All the tape drive components are highlighted in yellow. The beam direction is given by the red arrow. (b) Focus on the tape drive prototype: mechanical components of the tape drive (motor and pulleys) are highlighted in yellow, the Kapton® tape is highlighted in pink (with yellow arrows indicating the direction), the clean/dry unit highlighted in green, the piezoelectric

injector (PEI) unit (camera, PolyPico mini-head and LED) highlighted in blue and orthogonal view camera highlighted in light blue (blue arrow). (c) Close-up view of the PolyPico mini-head highlighted in purple. The cartridge is highlighted in orange (orange arrow). The micro-crystal slurry is ejected onto the side of the Kapton® tape and is brought to the interaction region with X-rays (red cross).

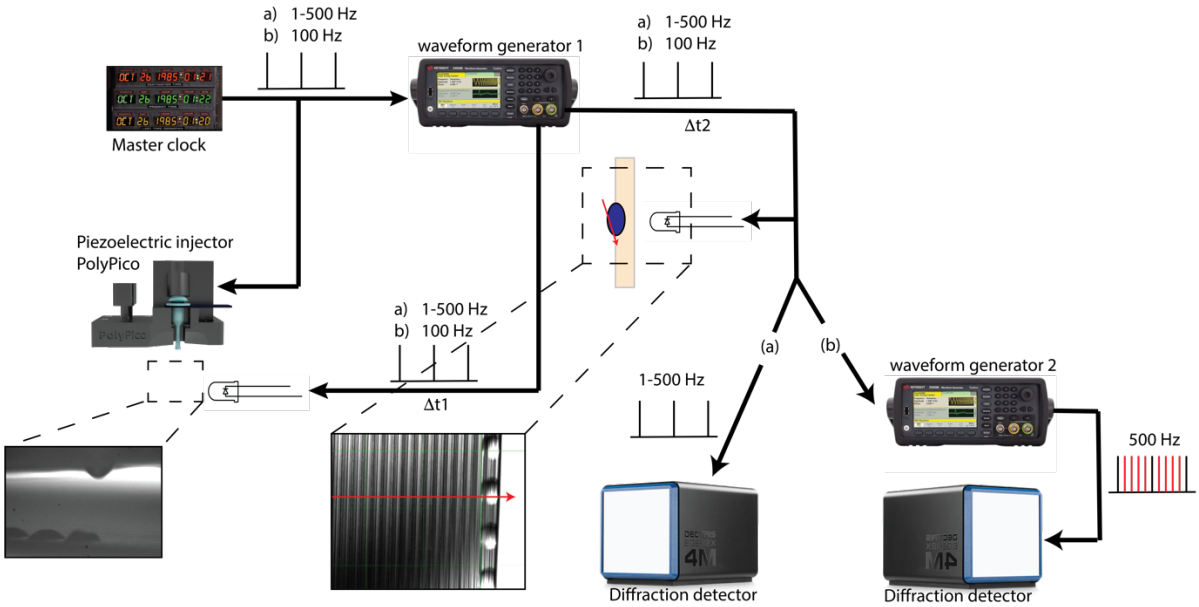

Figure 2 Triggering scheme of the tape drive and detector synchronisation. (a) The master clock is given by a signal generator which delivers TTL pulses at the desired frequency (up to 500 Hz). This TTL signal triggers the sample droplet ejection by the PEI. The master clock triggers at the same time "the waveform generator 1" which will produce 2 TTL signals at the same frequency with delay Δt1 and Δt2 respectively. The first TTL signal triggers the strobe LED attached to the PEI, Δt1is then adjusted allowing the visualization and the calibration of the droplet ejection onto the moving Kapton® tape. The second TTL signal triggers the strobe LED behind the tape at the interaction region with X-ray and the diffraction detector. By adjusting Δt2, the vertical position of the droplet on the tape is matched with the X-ray beam (red arrow), then the detector is triggered for acquiring diffraction data. (b) Same as (a) except that the master clock runs at 100 Hz, defining the droplet ejection at 100 Hz. A second waveform generator (2) is placed before the detector generating a 500 Hz signal. This mode of operation allows ejection of droplets at 100 Hz while acquiring images at 500 Hz.

(a)

(b)

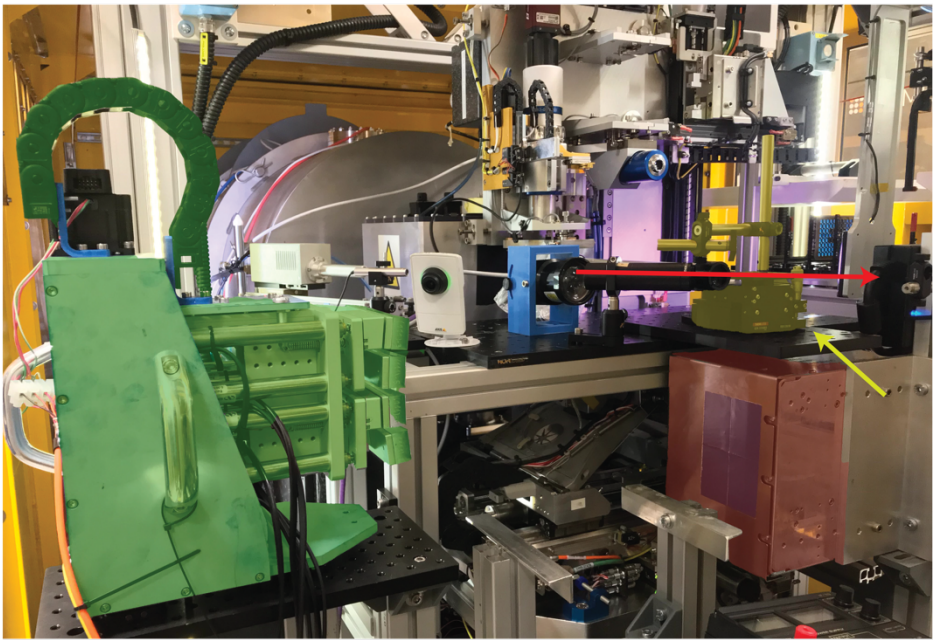

(c)

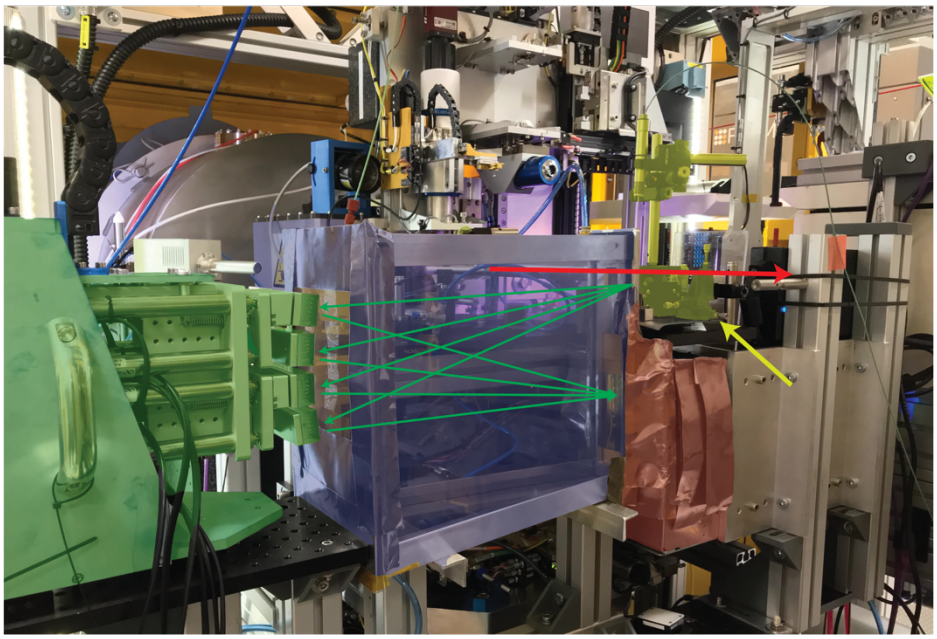

Figure 3 von Hamos XES spectrometer prototype installation at VMXi for Cu protein measurements. (a) A 4x1 bank of Si(111) analyser crystals with a 400 mm focal radius used to measure Cu $K\alpha_{1,2}$ XES data with the Si(444) reflection. (b) Setup without helium cone. The XES detector (Tristan1M) is highlighted in red, the analyser crystals bank is highlighted in green, and the sample delivery system is highlighted in yellow (yellow arrow). The X-ray beam direction is given by the red arrow. (c) Setup with helium cone, highlighted in blue, with emitted photon path showed in green arrows .

(a)

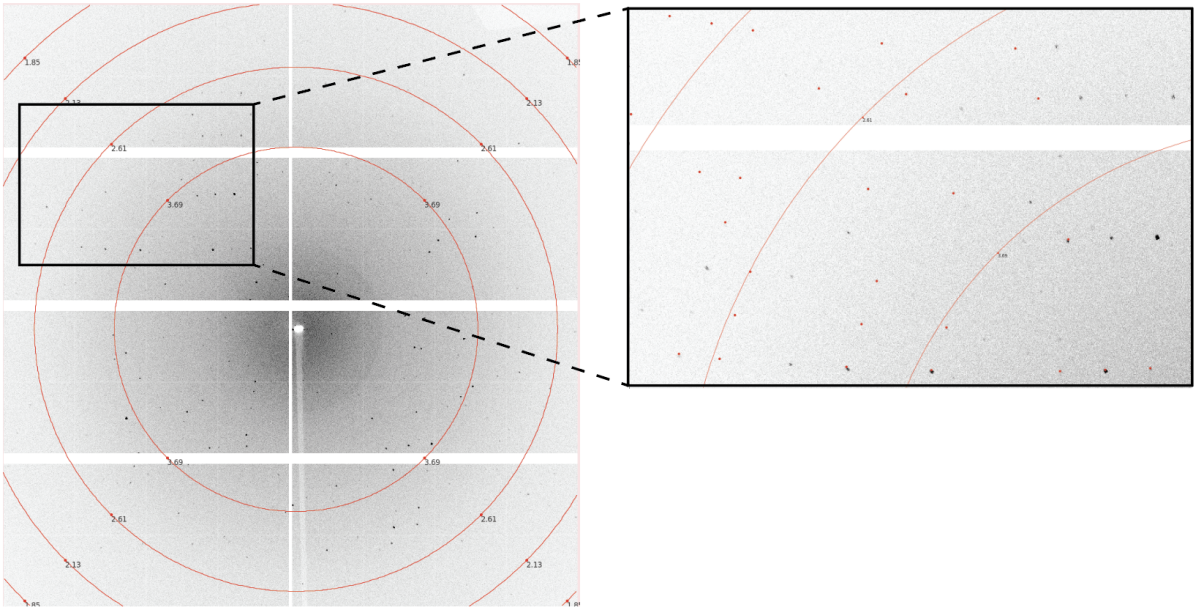

(b)

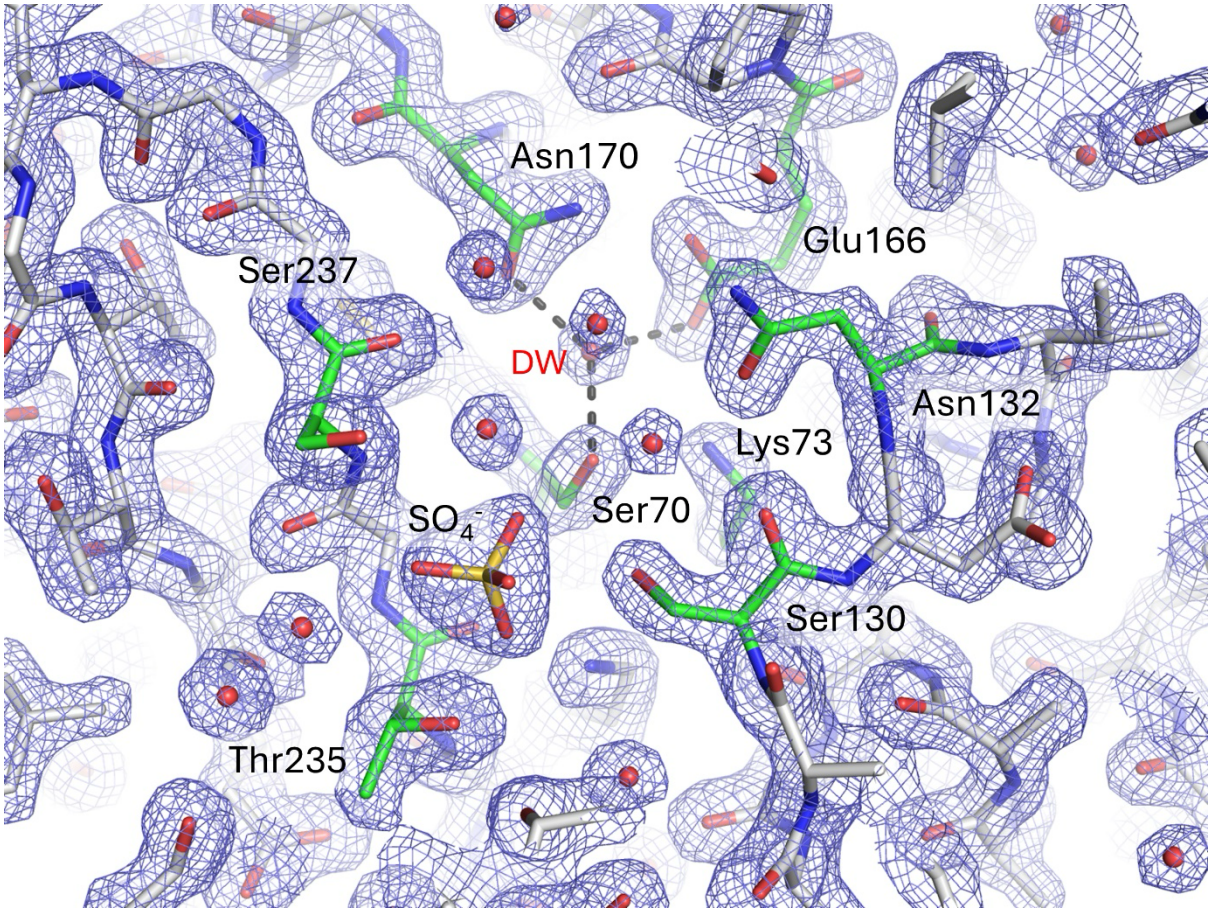

Figure 4 Serial synchrotron crystallography structure of serine beta lactamase CTX-M-15 from *Klebsiella pneumoniae* IS53 determined using tape drive at VMXi: (a) Diffraction pattern measured

from ~ 8 μm microcrystals within ~ 150 pL droplets (~ 66 μm diameter) on a moving tape at 0.25 m/s with 2 ms total exposure time during which crystals were in the X-ray beam for a maximum of ~ 700 μs. (b) The 2Fo-Fc electron density map at 1.83 Å resolution is shown as a blue mesh contoured at 1.2σ. The carbon atoms of key active site residues are coloured green and labelled. Sulphate (labelled) from the crystallisation condition is bound at the active site; the catalytic, deacylating water is labelled DW and hydrogen-bonded to Ser70, Glu166, and Asn170. The figure was created in PyMol (http://www.pymol.org/).

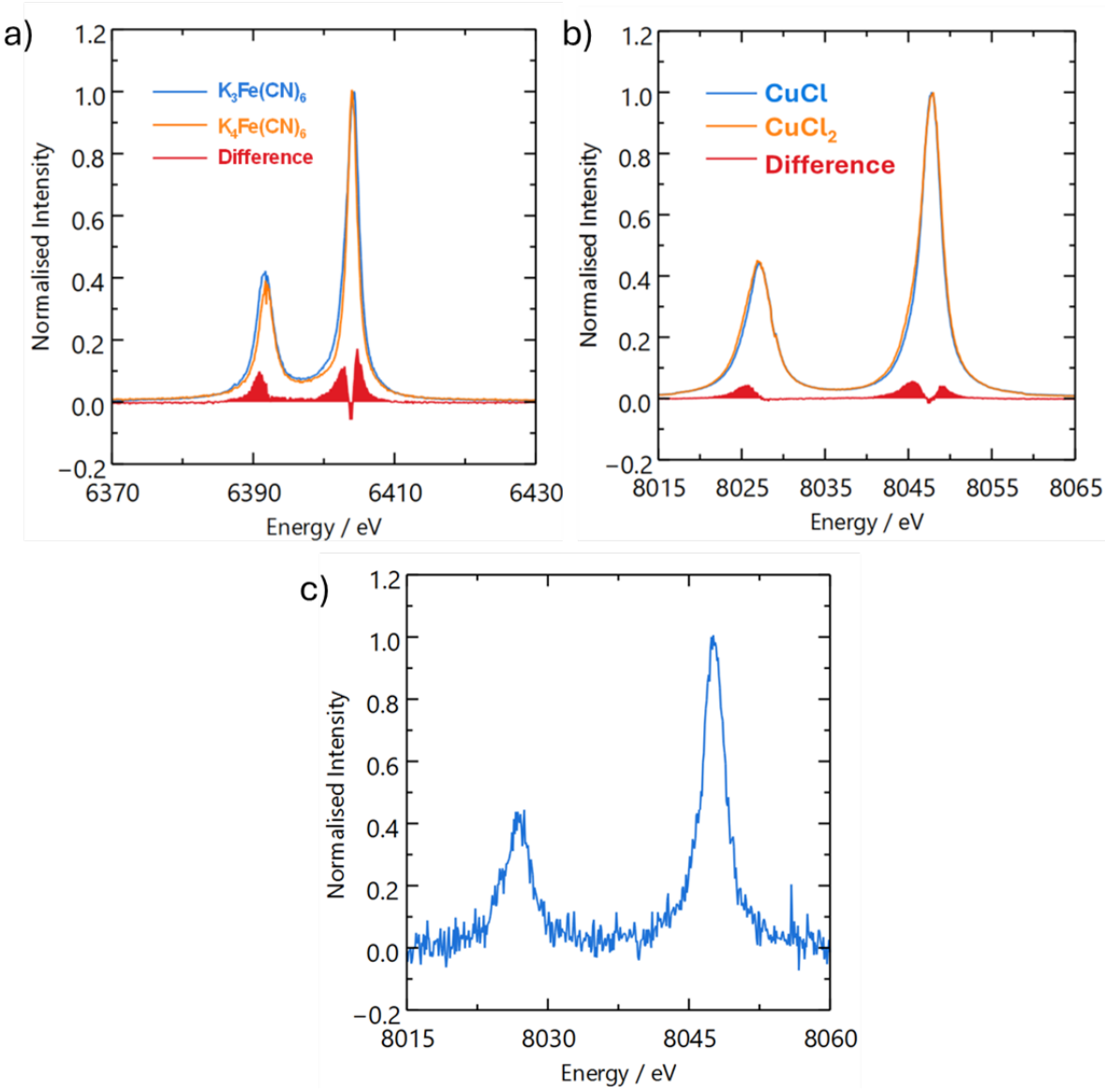

Figure 5 XES spectra. (a) $K\alpha_{1,2}$ XES of Fe salts ($K_3Fe(CN)_6$ and $K_4Fe(CN)_6$) and difference spectrum. (b) $K\alpha_{1,2}$ XES of Cu salts (CuCl and $CuCl_2$) and difference spectrum. (c) $K\alpha_{1,2}$ XES of AcNiR.

Table 1 Crystal exposure time to X-rays vs Tape speed

Linear tape speed in mm/s	Maximum time required for a 8 µm crystal to traverse a 10 µm X-ray beam (ms)	Dose* in kGy
10	2	34.7
25	0.8	13.9
50	0.4	6.9
100	0.2	3.5
200	0.1	1.7
500	0.04	0.7
1000	0.02	0.3

*Dose calculated with RADDOSE-3D (Bury et al., 2018; Paithankar & Garman, 2010) based on 8 x3x3 μm^3 CTX-M-15 crystal, and 100% transmission at 16 keV at VMXi with a flux of 2x1013 ph/s at VMXi .

Table 2 Diamond Light Source VMXi room temperature crystallographic data collection and refinement statistics for CTX-M-15 crystals

Resolution range (Å)	58.72 – 1.83 (1.86 – 1.83)
Space group	$P2_12_12_1$
Unit cell (Å, °)	44.01, 45.55, 117.44, 90, 90, 90
No. crystals merged	20556
Total reflections	2016541 (11570)
Unique reflections	21932 (1038)
Multiplicity	91.9 (11.1)
Completeness (%)	99.8 (98.2)
I/sigma(I)	9.2 (0.8)
R-split	0.117 (1.087)
$CC_{1/2}$	0.966 (0.305)
Refinement	
Resolution (Å)	58.72 – 1.83
No. reflections	21865
R_{work} / R_{free}	16.58/19.94
#. non-H atoms	
Protein	1976
Solvent	205
B-factors	
Protein	17.32
Solvent	28.75
R.m.s. deviations	
Bond lengths (Å)	0.005
Bond angles (°)	0.77
Ramachandran (%)	
Outliers	0.39
Favoured	98.44
PDB code	9YRD

Table 3 XES data measured at VMXi using a von Hamos spectrometer and a Merlin 1M or Tristan 1M detector.

Sample	Formal valence	Experimental $K\alpha_1$ FWHM /eV	COM / eV
$K_3Fe(CN)_6$	+3	2.5(1)	6399.0(1)
$K_4Fe(CN)_6$	+2	2.0(1)	6398.4(1)
CuCl	+1	2.8(1)	8046.3(1)
$CuCl_2$	+2	3.1(1)	8044.4(1)
AcNiR	+2	2.7(1)	8042.0(1)

Acknowledgements We gratefully acknowledge the work of colleagues at Diamond beyond the author list on projects related to the development of the tape drive and XES systems. We are grateful to beamline I24 for testing of copper nitrite reductase microcrystals. We are grateful to Dr. Roberto Alonso Mori for provision of Ge(440) analyser crystals.

Funding

This work was in part funded by the following grants to AMO: Wellcome Trust 210734/Z/18/Z; Royal Society Wolfson Fellowship RSWF\R2\182017. Support was also provided by the UKRI ISPF award 229 to AMO. This work is part of a project that has received funding from the European Research Council under the European Horizon 2020 research and innovation program (PREDACTED Advanced Grant Agreement no. 101021207) to JS. Research was supported by the BBSRC-funded South West Biosciences Doctoral Training Partnership (training grant reference BB/T008741/1, studentships to LP). CLT and JS thank the Medical Research Council for support through the grant MR/T016035/1. CLT thanks the University of Bath Prize Fellowship Scheme and the UK Medical Research Council for fellowship funding (UKRI330).

Data availability The authors declare no conflicts of interest. Coordinates and structure factors have been deposited in the Protein Data Bank with accession number 9YRD. XES spectra are made available on request.

REFERENCES

Adams, P. D., Afonine, P. V., Bunkoczi, G., Chen, V. B., Davis, I. W., Echols, N., . . . Zwart, P. H. (2010). PHENIX: a comprehensive Python-based system for macromolecular structure solution. *Acta Crystallogr D Biol Crystallogr*, *66*(Pt 2), 213-221. https://doi.org/10.1107/S0907444909052925

Aller, P., & Orville, A. M. (2021). Dynamic Structural Biology Experiments at XFEL or Synchrotron Sources. *Methods Mol Biol.*, *2305*, 203-228. https://doi.org/10.1007/978-1-0716-1406-8_11

Barends, T. R. M., Stauch, B., Cherezov, V., & Schlichting, I. (2022). Serial femtosecond crystallography. *Nat Rev Methods Primers*, *2*. https://doi.org/10.1038/s43586-022-00141-7

Beilsten-Edmands, J., Parkhurst, J. M., Winter, G., & Evans, G. (2024). Processing serial synchrotron crystallography diffraction data with DIALS. *Methods Enzymol*, *709*, 207-244. https://doi.org/10.1016/bs.mie.2024.10.004

Beitlich, T., Kuhnel, K., Schulze-Briese, C., Shoeman, R. L., & Schlichting, I. (2007). Cryoradiolytic reduction of crystalline heme proteins: analysis by UV-Vis spectroscopy and X-ray crystallography. *J Synchrotron Radiat*, *14*(Pt 1), 11-23. https://doi.org/10.1107/S0909049506049806

Beyerlein, K. R., Dierksmeyer, D., Mariani, V., Kuhn, M., Sarrou, I., Ottaviano, A., . . . Oberthuer, D. (2017). Mix-and-diffuse serial synchrotron crystallography. *IUCrJ*, *4*(Pt 6), 769-777. https://doi.org/10.1107/S2052252517013124

Birch, J., Kwan, T. O. C., Judge, P. J., Axford, D., Aller, P., Butryn, A., . . . Moraes, I. (2023). A versatile approach to high-density microcrystals in lipidic cubic phase for room-temperature serial crystallography. *J Appl Crystallogr*, *56*(Pt 5), 1361-1370. https://doi.org/10.1107/S1600576723006428

Branden, G., & Neutze, R. (2021). Advances and challenges in time-resolved macromolecular crystallography. *Science*, *373*(6558). https://doi.org/10.1126/science.aba0954

Bury, C. S., Brooks-Bartlett, J. C., Walsh, S. P., & Garman, E. F. (2018). Estimate your dose: RADDOSE-3D. *Protein Sci*, *27*(1), 217-228. https://doi.org/10.1002/pro.3302

Butryn, A., Simon, P. S., Aller, P., Hinchliffe, P., Massad, R. N., Leen, G., . . . Orville, A. M. (2021). An on-demand, drop-on-drop method for studying enzyme catalysis by serial crystallography. *Nat Commun*, *12*(1), 4461. https://doi.org/10.1038/s41467-021-24757-7

Chapman, H. N. (2019). X-Ray Free-Electron Lasers for the Structure and Dynamics of Macromolecules. *Annu Rev Biochem*, *88*, 35-58. https://doi.org/10.1146/annurev-biochem-013118-110744

Chen, V. B., Arendall, W. B., 3rd, Headd, J. J., Keedy, D. A., Immormino, R. M., Kapral, G. J., . . . Richardson, D. C. (2010). MolProbity: all-atom structure validation for macromolecular crystallography. *Acta Crystallogr D Biol Crystallogr*, *66*(Pt 1), 12-21. https://doi.org/10.1107/S0907444909042073

Chreifi, G., Baxter, E. L., Doukov, T., Cohen, A. E., McPhillips, S. E., Song, J., . . . Poulos, T. L. (2016). Crystal structure of the pristine peroxidase ferryl center and its relevance to proton-coupled electron transfer. *Proc Natl Acad Sci U S A*, *113*(5), 1226-1231. https://doi.org/10.1073/pnas.1521664113

Cutsail, G. I. I. I., & DeBeer, S. (2022). Challenges and Opportunities for Applications of Advanced X-ray Spectroscopy in Catalysis Research. *Acs Catalysis*, *12*(10), 5864-5886. https://doi.org/10.1021/acscatal.2c01016

Doak, R. B., Nass Kovacs, G., Gorel, A., Foucar, L., Barends, T. R. M., Grunbein, M. L., . . . Schlichting, I. (2018). Crystallography on a chip - without the chip: sheet-on-sheet sandwich. *Acta Crystallogr D Struct Biol*, *74*(Pt 10), 1000-1007. https://doi.org/10.1107/S2059798318011634

Emsley, P., & Cowtan, K. (2004). Coot: model-building tools for molecular graphics. *Acta Crystallogr D Biol Crystallogr*, *60*(Pt 12 Pt 1), 2126-2132. https://doi.org/10.1107/S0907444904019158

Fuller, F. D., Gul, S., Chatterjee, R., Burgie, E. S., Young, I. D., Lebrette, H., . . . Yano, J. (2017). Drop-on-demand sample delivery for studying biocatalysts in action at X-ray free-electron lasers. *Nat Methods*, *14*(4), 443-449. https://doi.org/10.1038/nmeth.4195

Glatzel, P., & Bergmann, U. (2005). High resolution 1s core hole X-ray spectroscopy in 3d transition metal complexes—electronic and structural information. *Coordination Chemistry Reviews*, *249*(1-2), 65-95.

Gonzalez, A., Krojer, T., Nan, J., Bjelcic, M., Aggarwal, S., Gorgisyan, I., . . . Thunnissen, M. (2025). Status and perspective of protein crystallography at the first multi-bend achromat based synchrotron MAX IV. *J Synchrotron Radiat*, *32*(Pt 3), 779-791. https://doi.org/10.1107/S1600577525002255

Hadimioglu, B., Stearns, R., & Ellson, R. (2016). Moving Liquids with Sound: The Physics of Acoustic Droplet Ejection for Robust Laboratory Automation in Life Sciences. *J Lab Autom*, *21*(1), 4-18. https://doi.org/10.1177/2211068215615096

Hajdu, J., Neutze, R., Sjogren, T., Edman, K., Szoke, A., Wilmouth, R. C., & Wilmot, C. M. (2000). Analyzing protein functions in four dimensions. *Nat Struct Biol*, *7*(11), 1006-1012. https://doi.org/10.1038/80911

Henkel, A., Galchenkova, M., Maracke, J., Yefanov, O., Klopprogge, B., Hakanpaa, J., . . . Oberthuer, D. (2023). JINXED: just in time crystallization for easy structure determination of biological macromolecules. *IUCrJ*, *10*(Pt 3), 253-260. https://doi.org/10.1107/S2052252523001653

Horrell, S., Antonyuk, S. V., Eady, R. R., Hasnain, S. S., Hough, M. A., & Strange, R. W. (2016). Serial crystallography captures enzyme catalysis in copper nitrite reductase at atomic resolution from one crystal. *IUCrJ*, *3*(Pt 4), 271-281. https://doi.org/10.1107/S205225251600823X

Horrell, S., Axford, D., Devenish, N. E., Ebrahim, A., Hough, M. A., Sherrell, D. A., . . . Owen, R. L. (2021). Fixed Target Serial Data Collection at Diamond Light Source. *J Vis Exp*(168). https://doi.org/10.3791/62200

Horrell, S., Kekilli, D., Sen, K., Owen, R. L., Dworkowski, F. S. N., Antonyuk, S. V., . . . Hough, M. A. (2018). Enzyme catalysis captured using multiple structures from one crystal at varying temperatures. *IUCrJ*, *5*(Pt 3), 283-292. https://doi.org/10.1107/S205225251800386X

Ibrahim, M., Fransson, T., Chatterjee, R., Cheah, M. H., Hussein, R., Lassalle, L., . . . Yano, J. (2020). Untangling the sequence of events during the S(2) --> S(3) transition in photosystem II and implications for the water oxidation mechanism. *Proc Natl Acad Sci U S A*, *117*(23), 12624-12635. https://doi.org/10.1073/pnas.2000529117

Jaho, S., Axford, D., Gu, D. H., Hough, M. A., & Owen, R. L. (2024). Use of fixed targets for serial crystallography. *Methods Enzymol*, *709*, 29-55. https://doi.org/10.1016/bs.mie.2024.10.002

Kamps, J., Bosman, R., Orville, A. M., & Aller, P. (2024). Sample efficient approaches in time-resolved X-ray serial crystallography and complementary X-ray emission spectroscopy using drop-on-demand tape-drive systems. *Methods Enzymol*, *709*, 57-103. https://doi.org/10.1016/bs.mie.2024.10.008

Lafuerza, S., Carlantuono, A., Retegan, M., & Glatzel, P. (2020). Chemical Sensitivity of Kbeta and Kalpha X-ray Emission from a Systematic Investigation of Iron Compounds. *Inorg Chem*, *59*(17), 12518-12535. https://doi.org/10.1021/acs.inorgchem.0c01620

Lebrette, H., Srinivas, V., John, J., Aurelius, O., Kumar, R., Lundin, D., . . . Högbom, M. (2023). Structure of a ribonucleotide reductase R2 protein radical. *Science*, *382*(6666), 109-113. https://doi.org/10.1126/science.adh8160

Mehrabi, P., Schulz, E. C., Agthe, M., Horrell, S., Bourenkov, G., von Stetten, D., . . . Miller, R. J. D. (2019). Liquid application method for time-resolved analyses by serial synchrotron crystallography. *Nat Methods*, *16*(10), 979-982. https://doi.org/10.1038/s41592-019-0553-1

Mehrabi, P., Schulz, E. C., Dsouza, R., Muller-Werkmeister, H. M., Tellkamp, F., Miller, R. J. D., & Pai, E. F. (2019). Time-resolved crystallography reveals allosteric communication aligned with molecular breathing. *Science*, *365*(6458), 1167-1170. https://doi.org/10.1126/science.aaw9904

Omar, D., Crevatin, G., Greer, A., Horswell, I., Spiers, J., Placket, R., . . . Tartoni, N. (2022). Tristan-A 10 Million Pixel Large Area Time Resolved Detector for Synchrotron Use. *Ieee Transactions on Nuclear Science*, *69*(10), 2188-2196. https://doi.org/10.1109/Tns.2022.3204064

Orlans, J., Rose, S. L., Ferguson, G., Oscarsson, M., Homs Puron, A., Beteva, A., . . . de Sanctis, D. (2025). Advancing macromolecular structure determination with microsecond X-ray pulses at a 4th generation synchrotron. *Commun Chem*, *8*(1), 6. https://doi.org/10.1038/s42004-024-01404-y

Orville, A. M. (2020). Recent results in time resolved serial femtosecond crystallography at XFELs. *Curr Opin Struct Biol*, *65*, 193-208. https://doi.org/10.1016/j.sbi.2020.08.011

Paithankar, K. S., & Garman, E. F. (2010). Know your dose: RADDOSE. *Acta Crystallogr D Biol Crystallogr*, *66*(Pt 4), 381-388. https://doi.org/10.1107/S0907444910006724

Pearson, A. R., & Mehrabi, P. (2020). Serial synchrotron crystallography for time-resolved structural biology. *Curr Opin Struct Biol*, *65*, 168-174. https://doi.org/10.1016/j.sbi.2020.06.019

Pfanzagl, V., Beale, J. H., Michlits, H., Schmidt, D., Gabler, T., Obinger, C., . . . Hofbauer, S. (2020). X-ray-induced photoreduction of heme metal centers rapidly induces active-site perturbations in a protein-independent manner. *J Biol Chem*, *295*(39), 13488-13501. https://doi.org/10.1074/jbc.RA120.014087

Plackett, R., Horswell, I., Gimenez, E. N., Marchal, J., Omar, D., & Tartoni, N. (2013). Merlin: a fast versatile readout system for Medipix3. *Journal of Instrumentation*, *8*. https://doi.org/Artn C01038

10.1088/1748-0221/8/01/C01038

Poikela, T., Plosila, J., Westerlund, T., Campbell, M., De Gaspari, M., Llopart, X., . . . Kruth, A. (2014). Timepix3: a 65K channel hybrid pixel readout chip with simultaneous ToA/ToT and sparse readout. *Journal of Instrumentation*, *9*. https://doi.org/Artn C05013

10.1088/1748-0221/9/05/C05013

Rabe, P., Kamps, J., Sutherlin, K. D., Linyard, J. D. S., Aller, P., Pham, C. C., . . . Schofield, C. J. (2021). X-ray free-electron laser studies reveal correlated motion during isopenicillin N synthase catalysis. *Sci Adv*, *7*(34). https://doi.org/10.1126/sciadv.abh0250

Roessler, C. G., Kuczewski, A., Stearns, R., Ellson, R., Olechno, J., Orville, A. M., . . . Heroux, A. (2013). Acoustic methods for high-throughput protein crystal mounting at next-generation macromolecular crystallographic beamlines. *J Synchrotron Radiat*, *20*(Pt 5), 805-808. https://doi.org/10.1107/S0909049513020372

Sanchez-Weatherby, J., Sandy, J., Mikolajek, H., Lobley, C. M. C., Mazzorana, M., Kelly, J., . . . Sorensen, T. L. M. (2019). VMXi: a fully automated, fully remote, high-flux in situ macromolecular crystallography beamline. *J Synchrotron Radiat*, *26*(Pt 1), 291-301. https://doi.org/10.1107/S1600577518015114

Sandy, J., Mikolajek, H., Thompson, A. J., Sanchez-Weatherby, J., & Hough, M. A. (2024). Crystallization and In Situ Room Temperature Data Collection Using the Crystallization Facility at Harwell and Beamline VMXi, Diamond Light Source. *J Vis Exp*(205). https://doi.org/10.3791/65964

Soares, A. S., Engel, M. A., Stearns, R., Datwani, S., Olechno, J., Ellson, R., . . . Orville, A. M. (2011). Acoustically mounted microcrystals yield high-resolution X-ray structures. *Biochemistry*, *50*(21), 4399-4401. https://doi.org/10.1021/bi200549x

Srinivas, V., Banerjee, R., Lebrette, H., Jones, J. C., Aurelius, O., Kim, I. S., . . . Hogbom, M. (2020). High-Resolution XFEL Structure of the Soluble Methane Monooxygenase Hydroxylase Complex with its Regulatory Component at Ambient Temperature in Two Oxidation States. *J Am Chem Soc*, *142*(33), 14249-14266. https://doi.org/10.1021/jacs.0c05613

Thompson, A., Attwood, D., Gullikson, E., Howells, M., Kim, K. J., Kirz, J., . . . Winick, H. (2009). X-RAY DATA BOOKLET. *Lawrence Berkeley National Laboratory, University of California, Berkeley, CA 94720*.

Tooke, C. L., Hinchliffe, P., Lang, P. A., Mulholland, A. J., Brem, J., Schofield, C. J., & Spencer, J. (2019). Molecular Basis of Class A beta-Lactamase Inhibition by Relebactam. *Antimicrob Agents Chemother*, *63*(10). https://doi.org/10.1128/AAC.00564-19

Weierstall, U., James, D., Wang, C., White, T. A., Wang, D., Liu, W., . . . Cherezov, V. (2014). Lipidic cubic phase injector facilitates membrane protein serial femtosecond crystallography. *Nat Commun*, *5*, 3309. https://doi.org/10.1038/ncomms4309

Zielinski, K. A., Prester, A., Andaleeb, H., Bui, S., Yefanov, O., Catapano, L., . . . Oberthuer, D. (2022). Rapid and efficient room-temperature serial synchrotron crystallography using the CFEL TapeDrive. *IUCrJ*, *9*(Pt 6), 778-791. https://doi.org/10.1107/S2052252522010193